DOI: https://doi.org/10.53256/COSE_240203

Neural Network-Based Nonlinear Coastal Wave Forecasting Using Hindcast Data and Phase-Resolving Wave Modelling

W. W. Wang[a,*] and H. Bihs[a]
[a]*Civil and Environmental Engineering, Norwegian University of Science and Technology, Trondheim, Norway*

[*]*Corresponding author: Widar Weizhi Wang, widar.w.wang@ntnu.no*

ABSTRACT: As ocean waves approach the shore and propagate over complex coastal topo-bathymetry, the wave field becomes increasingly inhomogeneous and nonlinear. Such nonlinear behaviour poses significant challenges for phase-averaged wave models, particularly in representing wave transformation processes such as diffraction, for which phase-resolving models are often required. With the growing availability of hindcast datasets, data-driven approaches—enabled by recent advances in machine-learning techniques, including neural networks—have increasingly been applied to offshore wave forecasting. In this study, a feed-forward multilayer perceptron (MLP) is employed to establish a nonlinear relationship between offshore and nearshore wave conditions, using phase-resolving wave model outputs as training data. A suite of phase-resolving numerical simulations, conducted under varying offshore wave conditions, is used to generate the training dataset. By combining machine-learning techniques with phase-resolving simulations, the proposed approach yields accurate predictions of wave heights in shoaling and diffraction zones, as well as wave forces acting on the shoal, and demonstrates clear advantages over linear and polynomial regression methods at the test site. Furthermore, the study investigates the coupling of long short-term memory (LSTM)-based offshore wave forecasting with the MLP-based offshore-to-nearshore correlation. The results indicate that this hybrid framework represents a promising pathway towards reliable, site-specific coastal wave forecasting.

KEYWORDS: phase-resolving modelling, numerical simulation, machine learning, coastal wave transformation

1 INTRODUCTION

As ocean waves propagate from deep offshore waters towards coastal regions, they interact with varying seabed topography and irregular coastlines, leading to complex and nonlinear wave transformations such as shoaling, refraction, diffraction, and breaking. These nonlinear processes in coastal waters make the accurate description and prediction of nearshore wave conditions particularly challenging. Well-established offshore wave spectra, such as the JONSWAP spectrum (Hasselmann et al., 1973), often fail to adequately represent coastal wave fields. Attempts to incorporate shallow-water effects into spectral formulations have been made, for example through the TMA spectrum (Hughes, 1984), which modifies the JONSWAP spectrum. However, such formulations are typically limited to constant water-depth scenarios and do not fully account for spatially varying bathymetry.

As coastal blue-economy activities continue to expand—including offshore wind farms, aquaculture, maritime transport, coastal infrastructure, and climate-change adaptation and protection—it has become increasingly important to characterize coastal wave conditions with greater accuracy and detail.

Moving beyond analytical wave descriptions, spectral wave models such as SWAN (Booij et al., 1999) are widely used for offshore and coastal wave prediction. However, within the phase-averaged framework, approximations of nonlinear coastal wave transformations—particularly diffraction—are often inadequate (Holthuijsen et al., 2003). This limitation can lead to the underestimation of wave energy in diffraction-dominated regions and inaccurate representations of coastal wave spectra (Wang et al., 2022). To capture nonlinear wave processes with higher fidelity, phase-resolving wave models are frequently required.

Among the most widely used phase-resolving models are: shallow-water equation (SWE)-based models, such as Boussinesq-type formulations (Madsen et al., 1991; Madsen et al., 1998) and SWE models incorporating quadratic non-hydrostatic pressure corrections (Wang et al., 2020); fully nonlinear potential flow (FNPF) models, including high-order spectral (HOS) models (Ducrozet et al., 2012) and finite-difference-based formulations (Engsig-Karup et al., 2009; Bihs et al., 2020); and three-dimensional non-hydrostatic models (Zijlema et al., 2011; Bihs et al., 2024). Based on a free-surface- and bathymetry-following σ-grid—where the vertical coordinate is normalized between 0 at the seabed and 1 at the free surface—the fully nonlinear potential flow model REEF3D::FNPF (Wang et al., 2022) introduces a novel coastline treatment based on a combined wetting–drying and level-set approach. Together with flexible wave-breaking detection and dissipation algorithms, the model has demonstrated its ability to efficiently and reliably simulate large-scale coastal wave propagation and transformation over strongly varying bathymetry.

Although phase-resolving models can accurately represent coastal wave nonlinearity, they typically require substantial computational resources and simulation time. For certain applications, faster predictions of coastal wave parameters—or even wave-induced loads—are desirable, for example in fairway and harbour operation optimisation or in the development of digital twins for coastal structures. With the growing availability of both measured and numerically simulated datasets, data-driven approaches have emerged as viable alternatives. Recent developments have seen an increasing application of machine-learning (ML) techniques in coastal and ocean engineering. Based on buoy measurements or hindcast datasets, several studies have attempted to predict future wave conditions using ML methods (James et al., 2018; Feng et al., 2022; Minuzzi and Farina, 2023). More recently, Harris (2024) presented a faster-than-real-time, phase-resolving, data-driven framework for wave propagation and wave–structure interaction. However, most existing studies focus on offshore conditions, while wave transformation processes in coastal waters remain less explored.

In this study, a combined numerical modelling and machine-learning approach is proposed to correlate offshore wave conditions with nearshore wave parameters. The phase-resolving model REEF3D::FNPF is used to generate synthetic coastal wave datasets under varying offshore wave inputs. A feed-forward multilayer perceptron (MLP) neural network is then developed to establish a relationship between offshore wave parameters and nearshore wave heights, as well as wave forces acting on a cylindrical structure located in both shoaling and diffraction regions. Although the primary focus is on offshore–coastal correlation, the study also investigates the potential coupling of the MLP framework with a long short-term memory (LSTM) recurrent neural network for offshore wave prediction, offering a promising pathway towards efficient and reliable forecasting of coastal wave conditions and associated wave loads.

2 NUMERICAL MODEL

The phase-resolving numerical wave model employed in this study is the fully nonlinear potential flow model REEF3D::FNPF (Wang et al., 2022). The governing equation is the Laplace equation, given by Eq. (1):

$$\frac{\partial^2 \phi}{\partial x^2} + \frac{\partial^2 \phi}{\partial y^2} + \frac{\partial^2 \phi}{\partial z^2} = 0 \tag{1}$$

The velocity potential ϕ is obtained by solving Eq. (1) subject to fully nonlinear boundary conditions. These include the kinematic and dynamic free-surface boundary conditions, given in Eqs. (2) and (3), respectively, and the bottom boundary condition, given in Eq. (4):

$$\frac{\partial \eta}{\partial t} = -\frac{\partial \eta}{\partial x}\frac{\partial \tilde{\phi}}{\partial x} - \frac{\partial \eta}{\partial y}\frac{\partial \tilde{\phi}}{\partial y} + \tilde{w}\left(1 + \left(\frac{\partial \eta}{\partial x}\right)^2 + \left(\frac{\partial \eta}{\partial y}\right)^2\right) \tag{2}$$

$$\frac{\partial \tilde{\phi}}{\partial t} = -\frac{1}{2}\left(\left(\frac{\partial \tilde{\phi}}{\partial x}\right)^2 + \left(\frac{\partial \tilde{\phi}}{\partial y}\right)^2\right) + \frac{1}{2}\widetilde{w^2}\left(1 + \left(\frac{\partial \eta}{\partial x}\right)^2 + \left(\frac{\partial \eta}{\partial y}\right)^2\right) - g \tag{3}$$

$$\frac{\partial \phi}{\partial z} + \frac{\partial h}{\partial x}\frac{\partial \phi}{\partial x} + \frac{\partial h}{\partial y}\frac{\partial \phi}{\partial y} = 0 \tag{4}$$

In these boundary conditions, η denotes the free-surface elevation, h is the still-water depth, $\tilde{\phi}$and $\tilde{w}$represent the velocity potential and vertical particle velocity evaluated at the free surface, respectively, and g is the gravitational acceleration.

The governing equation and boundary conditions are solved using a finite-difference method on a structured horizontal grid, combined with a σ-coordinate system in the vertical direction, defined as:

$$\sigma = \frac{z+h(x)}{\eta(x,t)+h(x)} \quad (5)$$

The Laplace equation is solved using a conjugate-gradient solver from the **hypre** library (van der Vorst, 1992), combined with a parallelized geometric multigrid preconditioner. Spatial discretization of the governing equations and boundary conditions is performed using a fifth-order Hamilton–Jacobi weighted essentially non-oscillatory (WENO) scheme (Jiang and Shu, 1996), while time integration is carried out using a third-order total variation diminishing (TVD) Runge–Kutta scheme (Shu and Osher, 1988).

Wave generation is achieved through a relaxation-zone method (Larsen and Dancy, 1983). Wetting–drying processes and coastline detection are handled using a level-set-based algorithm, as described by Wang et al. (2022). Depth-induced and steepness-induced wave breaking are detected based on velocity and steepness criteria (Smit et al., 2013), and wave energy dissipation due to breaking is approximated using an artificial viscosity approach (Baquet et al., 2017). The solver is fully parallelized using the Message Passing Interface (MPI) protocol.

An Arbitrary Lagrangian–Eulerian (ALE) method (Pákozdi et al., 2022) is incorporated into the numerical wave model to enable efficient wave-force calculations. In this approach, the motion of fluid particles and the moving computational grid are synchronized, allowing the numerically resolved nonlinear wave kinematics—such as particle velocities and accelerations during wave transformation—to be directly used in the Morison equation for calculating wave loads on cylindrical structures. The formulation for the wave force in the x-direction is given by Eq. (6):

$$F_x = \rho(h+\eta) \left[\int_0^1 C_M a_x A \, d\sigma + \frac{1}{2}\int_0^1 C_D u|u| \, D d\sigma\right] \quad (6)$$

Here, C_M and C_D are the inertia and drag coefficients, respectively; $A$is the cross-sectional area of the structure; $D$is the cylinder diameter; and a_x and u denote the particle acceleration and velocity in the x-direction.

3 MACHINE LEARNING ALGORITHMS

A feedforward multilayer perceptron (MLP) is employed to establish the relationship between offshore wave parameters and nearshore wave characteristics, including wave forces. Simulated significant wave heights and wave-induced forces obtained from the numerical wave model are used as input–output pairs for training the MLP. Prior to training, all simulated data are normalized using a Min–Max scaling procedure to ensure numerical stability and efficient convergence.
The dataset is randomly divided into training and validation subsets using an 80:20 split. The MLP architecture consists of two fully connected hidden layers with 64 and 32 neurons, respectively, followed by an output layer. The rectified linear unit (ReLU) is adopted as the activation function, while the adaptive moment estimation (Adam) algorithm is used for optimization of the network weights and biases. Model performance is evaluated using the mean squared error (MSE) as the loss function.
To enable offshore wave forecasting based on time-series data, a long short-term memory (LSTM) network is also employed. LSTM networks represent an advanced form of recurrent neural networks (RNNs) that are well suited for learning long-term temporal dependencies in sequential datasets. In this study, the time history of significant wave heights from January to November 2024, obtained from the NORA3 hindcast dataset at an offshore location outside the study site, is used to train the LSTM model, which is subsequently applied to predict wave heights for December 2024.
The LSTM architecture consists of two stacked LSTM layers, each with 50 units, followed by a dense output layer. Similar to the MLP configuration, the Adam optimizer, ReLU activation function, and an MSE-based loss function are adopted. The LSTM implementation is based on the open-source framework developed by the Norwegian Meteorological Institute (https://github.com/MET-OM/metocean-ml).

The interconnections and overall workflow between the numerical wave model and the machine learning components are summarized in Fig. 1.

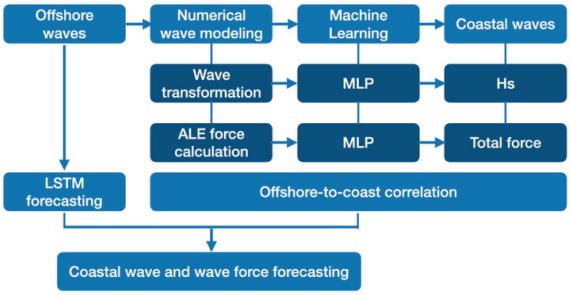

Figure 1. Workflow of the coupled numerical wave model and machine learning framework for coastal wave and wave-force prediction.

4 CASE DESCRIPTION

The study site is located in southern Norway, near the city of Kristiansand. The area of interest comprises the surrounding waters near the island of Store Lyngholmen, which is centred in Fig. 2. The dominant incident waves propagate from the southern boundary of the domain. A navigation tower is planned to be constructed on a shoal south of Store Lyngholmen, indicated as location G1. An anchorage area is situated on the lee side of the island and is denoted as location G2.

The phase-resolving numerical wave tank (NWT) reproduces the bathymetry of the study domain, as shown in Fig. 2. The blue box in Fig. 2 represents the relaxation zone used for wave generation, while the three orange boxes correspond to relaxation zones functioning as numerical beaches to attenuate undesired wave reflections at the domain boundaries.

The imposed irregular waves follow a JONSWAP spectrum with a constant peak period of $T_p = 12$s and a varying significant wave height H_s, ranging from 0.5 m to 10.4 m in increments of 0.1 m. This configuration results in a total of 100 numerical simulations representing different offshore wave conditions. The simulated significant wave heights at locations G1 and G2 are used to train an MLP model for wave height prediction. In addition, the simulated maximum total wave force at location G1 is employed to train a separate MLP model for wave force prediction.

For the idealised cylindrical navigation tower at G1, a diameter of 3 m is assumed. The inertia and drag coefficients used in the force calculations are set to 1.5 and 0.9, respectively.

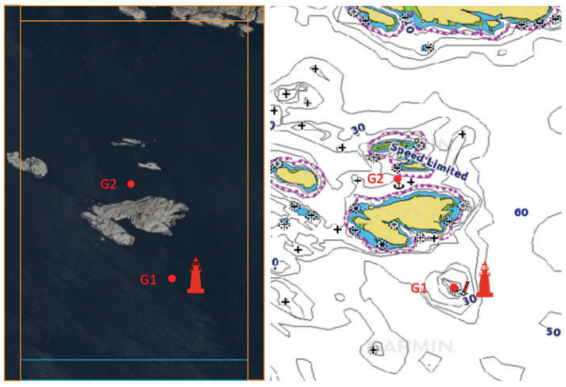

Figure 2. Illustration of the study site, including a satellite image and a bathymetric map. Locations of interest are marked as G1 and G2. G1 is located on a shoal where a navigation tower is planned, while G2 is situated at an anchorage on the lee side of Store Lyngholmen. The blue box indicates the wave generation zone, and the orange boxes represent numerical beach zones.

5 RESULTS AND DISCUSSIONS

Twenty percent of the 100 numerical simulations were used to validate the MLP-based predictions. The MLP-predicted significant wave heights at location G1 (shoaling region), represented by red crosses, are compared with the simulated values (blue dots) for the 20 validation cases in Fig. 3. The x-axis represents the offshore input significant wave height H_s used in the numerical simulations, while the y-axis shows the corresponding simulated and predicted H_s values at G1.

The results indicate that the MLP-predicted significant wave heights closely match those obtained from the phase-resolving simulations across the full range of offshore input wave heights. The machine learning model also reproduces the overall variation trend with high fidelity. In contrast, the linear regression model (cyan dotted line in Fig. 3) fails to accurately predict both the magnitude of H_s and its nonlinear trend. The polynomial regression model (purple dotted curve in Fig. 3), however, provides a comparatively good approximation of the significant wave heights.

Quantitatively, the mean squared error (MSE) of the MLP predictions for the 20 validation cases is 0.141 m, which is higher than that of the polynomial regression (0.054 m). As expected, the linear regression yields the largest error, with an MSE of 0.424 m.

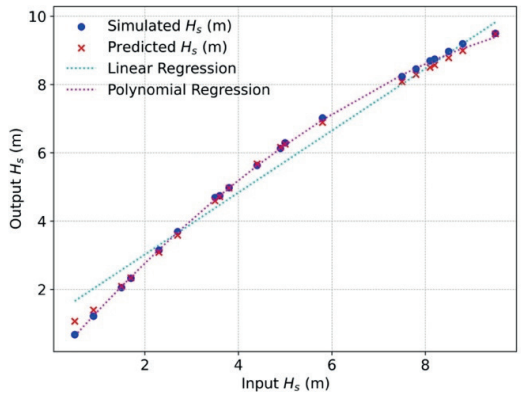

Figure 3. Comparison of simulated significant wave heights at G1 (shoaling region) with predictions obtained using MLP, linear regression, and polynomial regression.

A similar validation exercise was conducted for the diffracted wave field at location G2, as shown in Fig. 4. The observations are consistent with those for the shoaling region. Both the MLP and polynomial regression models accurately predict the magnitude and trend of the diffracted waves, whereas the linear regression again fails to capture the underlying behavior of the wave field. In this case, the MSE values are 0.027 m for the MLP, 0.068 m for linear regression, and 0.013 m for polynomial regression.

More pronounced differences among the prediction methods are observed for the maximum total wave forces acting on the cylindrical structure at G1. As shown in Fig. 5, the total wave force exhibits a stronger nonlinear relationship with offshore wave height than the significant wave height. Initially, the force increases rapidly with increasing offshore H_s; beyond approximately 4 m offshore H_s, the growth rate decreases markedly. This nonlinear behavior can be attributed to premature wave breaking in front of the shoal as offshore wave heights increase.

In this regime, the MLP demonstrates a clear advantage in capturing the complex transition in the physical wave transformation process. The MLP-predicted maximum total wave forces agree well with both the simulated magnitudes and the observed trend. Neither the linear regression nor the polynomial regression adequately reproduces this nonlinear behavior. The MLP approach yields the lowest MSE of 95.89 kN, compared to 342 kN for linear regression and 161 kN for polynomial regression.

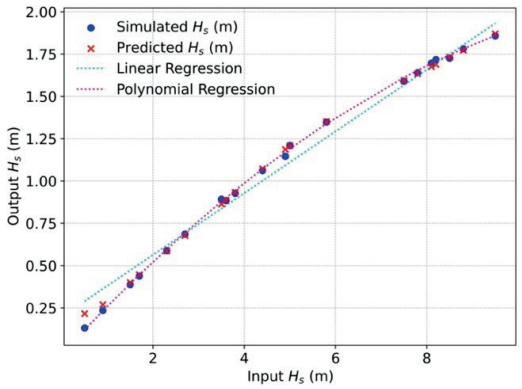

Figure 4. Comparison of simulated significant wave heights at G2 (diffraction region) with predictions obtained using MLP, linear regression, and polynomial regression.

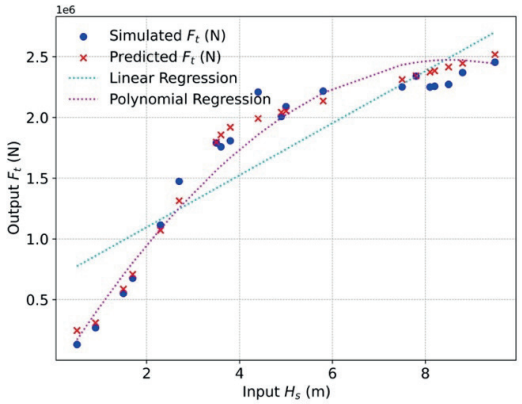

Figure 5. Comparison of simulated maximum total wave forces at G1 (shoaling region) with predictions obtained using MLP, linear regression, and polynomial regression.

Overall, the MLP algorithm provides consistent and reliable predictions for shoaling waves, diffracted waves, and maximum total wave forces. This demonstrates its capability for rapid prediction of coastal wave parameters and wave-induced forces based solely on offshore wave inputs at the study site.

To enable coastal wave forecasting, an LSTM-based model was employed to predict offshore wave conditions using existing hindcast data. Hourly significant wave height time series from an offshore location south of Store Lyngholmen (longitude 7.9293369° E, latitude 58.0167552° N) between January and November 2024 were used to train the LSTM model, which was then applied to predict the wave height time series for December 2024. The predicted H_s values are validated against the corresponding hindcast data for December 2024, as shown in Fig. 6.

The LSTM model successfully captures the general temporal evolution of the significant wave height throughout December. The predicted significant wave height at 23:00 on 31 December 2024 is 3.76 m.

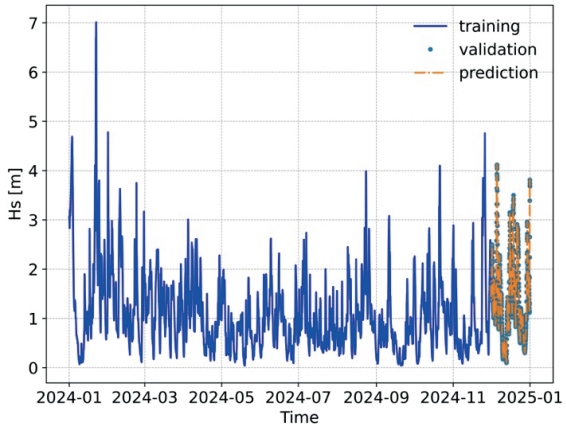

Figure 6. LSTM-based prediction of the significant wave height time series for December 2024 (dash–dotted orange line), validated against hindcast data for December (blue dots), using training data from January to November 2024 (solid blue line).

A new phase-resolving simulation was subsequently performed using the predicted offshore significant wave height of 3.76 m as input. The simulated free surface elevation within the numerical wave tank is shown in Fig. 7. Pronounced wave shoaling is observed, while diffracted waves propagate around both the western and eastern sides of Store Lyngholmen and converge in the lee of the island at the anchorage location.

The MLP-predicted significant wave heights at G1 and G2 are 4.954 m and 0.922 m, respectively. The corresponding simulated values are 4.939 m and 0.9378 m, yielding percentage errors of only 0.3% and 1.7%. Since the offshore input wave height lies within the range of the training data, this strong agreement is expected. However, the predicted maximum total wave force is 19,001 kN, which is approximately 10% lower than the simulated value. As the input wave height is close to the wave-breaking transition regime, the wave kinematics become more irregular and strongly nonlinear, making accurate force prediction more challenging in this range.

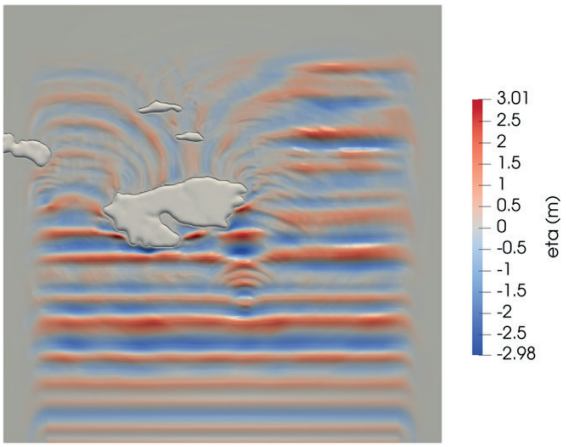

Figure 7. Free surface elevation from the phase-resolving simulation using the predicted offshore significant wave height of 3.76 m on 31 December 2024.

CONCLUSIONS

This study presents a case study demonstrating a hybrid framework that integrates a phase-resolving numerical wave model, hindcast data, and machine-learning techniques. A phase-resolving numerical wave tank (NWT) was used to generate training data for a multi-layer perceptron (MLP), enabling the establishment of a robust correlation between offshore and coastal wave conditions that captures the nonlinear nature of coastal wave transformation. Hindcast data were further employed to train a long short-term memory (LSTM) model for short-term offshore sea-state prediction. When combined, these models provide a computationally efficient approach for rapid forecasting of coastal wave conditions.

The coupled NWT–MLP framework successfully reproduces the key physical processes governing wave shoaling, diffraction, and wave-induced forces acting on a cylindrical structure. Its advantages are particularly evident in the prediction of wave forces, where it clearly outperforms simpler surrogate models such as linear and polynomial regressions. Although further investigation is required—particularly regarding the sensitivity to machine-learning architectures, training data volume, and input parameter selection—the results demonstrate the feasibility and practical potential of the proposed approach for coastal engineering applications, including real-time forecasting and decision support.

ACKNOWLEDGEMENTS

The authors acknowledge funding from the European Union (ERC, PARTRES, grant agreement No. 101045646). The views and opinions expressed in this work are those of the authors only and do not necessarily reflect those of the European Union or the European Research Council Executive Agency. Neither the European Union nor the granting authority can be held responsible for them. The numerical simulations were performed on the Betzy supercomputer, provided by Sigma2 – the National Infrastructure for High-Performance Computing and Data Storage in Norway.

REFERENCES

Baquet, A., Kim, J., Huang, Z.J. (2017) Numerical modeling using CFD and potential wave theory for three-hour nonlinear irregular wave simulations. In: International Conference on Offshore Mechanics and Arctic Engineering. Vol. 1: Offshore Technology: V001T01A002

Bihs, H., Wang, W., Pákozdi, C., Kamath, A. (2020) REEF3D::FNPF—A Flexible Fully Nonlinear Potential Flow Solver, Journal of Offshore Mechanics and Arctic Engineering 142 (4): 041902.

Bihs, H., Ehlers R., Wang W. (2024) A Shock-absorbing non-hydrostatic Navier-Stokes solver on σ-grids for wave modeling over irregular topography, 43rd International Conference on Ocean, Offshore & Arctic Engineering, Singapore, Volume 6: Polar and Arctic Sciences and Technology; CFD, FSI, and AI: V006T08A016

Booij, N., Ris, R. C., Holthuijsen, L. H. (1999) A third-generation wave model for coastal regions: 1. Model description and validation, Journal of Geophysical Research: Oceans 104 (C4): 7649–7666.

Ducrozet, G., Bonnefoy, F. e. l., Le Touzé, D., Ferrant, P. (2012) A modified High-Order Spectral method for wavemaker modeling in a numerical wave tank, European Journal of Mechanics - B/Fluids 34: 19-34

Engsig-Karup, A., Bingham, H., Lindberg, O. (2009) An efficient flexible-order model for 3D nonlinear water waves, Journal of Computational Physics 228: 2100–2118.

Feng, Z., Hu, P., Li, S. and Mo, D. (2022) Prediction of significant wave height in offshore China based on the machine learning method. Journal of Marine Science and Engineering 10 (6): 836

Haakenstad, H., Breivik, Ø., Furevik, B. R., Reistad, M., Bohlinger, P., Aarnes, O. J. (2021) NORA3: A nonhydrostatic high-resolution hindcast of the North Sea, the Norwegian Sea, and the Barents Sea, Journal of Applied Meteorology and Climatology 60 (10): 1443–1464

Harris, J, C. (2024) Faster than real-time, phase-resolving, data-driven model of wave propagation and wave–structure interaction. Applied Ocean Research 154: 104291

Hasselmann, K., Barnett, T., Bouws, E., Carlson, H., Cartwright, D.. Enke, K., Ewing, J., Gienapp, H., Hasselmann, D., Kruseman, P., Meerburg, A., Müller, P., Olbers, D., Richter, K., Sell, W., Walden, H. (1973) Measurements of wind-wave growth and swell decay during the Joint North Sea Wave Project (JONSWAP), Ergänzungsheft zur Deutschen Hydrographischen Zeitschrift, Reihe A 12 (8): 1–95.

Holthuijsen, L., Herman, A., Booij, N. (2003) Phase-decoupled refraction–diffraction for spectral wave models, Coastal Engineering 49 (4): 291–305.

Hughes, S. A. (1984) The TMA shallow-water spectrum description and applications, Coastal Engineering Research Center, Vicksburg, Mississippi, U.S.A. Tech. Rep.: CERC-84-7

James, S. C., Zhang, Y. and O'Donncha, F. (2018) A machine learning framework to forecast wave conditions. Coastal Engineering 137: p. 1–10.

Jeschke, A., Pedersen, G. K., Vater, S., Behrens, J. (2017) Depth-averaged non-hydrostatic extension for shallow water equations with quadratic vertical pressure profile: equivalence to Boussinesq-type equations, International Journal for Numerical Methods in Fluids 84 (10): 569–583

Jiang, G. S., Shu, C. W., (1996) Efficient implementation of weighted ENO schemes. J. Comput. Phys. 126: 202–228.

Larsen, J., Dancy, H., (1983) Open boundaries in short wave simulations — A new approach. Coast. Eng. 7 (3): 285–297.

Madsen, P. A., Murray, R., Sørensen, O. R. (1991) A new form of the Boussinesq equations with improved linear dispersion characteristics, Coastal Engineering 15: 371–388.

Madsen, P. A., Schäffer, H. A. (1998) Higher-order Boussinesq-type equations for surface gravity waves: derivation and analysis, Philosophical Transactions of the Royal Society of London. Series A: Mathematical, Physical and Engineering Sciences 356 (1749): 3123–3181.

Minuzzi, F. C., Farina, L. (2023) A deep learning approach to predict significant wave height using long short-term memory. Ocean Modelling 181: 102151

Pákozdi, C., Kamath, A., Wang, W. and Bihs, H. (2022) Application of Arbitrary Lagrangian–Eulerian strips with fully nonlinear wave kinematics for force estimation. Marine Structures 83: 103190.

Shu, C. W., Osher, S., (1988) Efficient implementation of essentially non-oscillatory shock capturing schemes. J. Comput. Phys. 77: 439–471.

Smit, P., Zijlema, M., Stelling, G. (2013) Depth-induced wave breaking in a nonhydrostatic, near-shore wave model. Coast. Eng. 76: 1–16.

Wang, W., Pákozdi, C., Kamath, A., Fouques, S. and Bihs, H. (2022) A flexible fully nonlinear potential flow model for wave propagation over the complex topography of the Norwegian coast. Applied Ocean Research 122: 103103.

van der Vorst, H. (1992) BiCGStab: a fast and smoothly converging variant of Bi-CG for the solution of nonsymmetric linear systems. SIAM J. Sci. Comput. 13: 631–644.

Wang, W., Martin, T., Kamath, A., Bihs, H. (2020) An Improved Depth-Averaged Non-Hydrostatic Shallow Water Model with Quadratic Pressure Approximation, International Journal for Numerical Methods in Fluids 92: 803–824.

Zijlema, M., Stelling, G., Smit, P. (2011) SWASH: An operational public domain code for simulating wave fields and rapidly varied flows in coastal waters, Coastal Engineering 58 (10): 992–1012.